

Computational screening of core@shell nanoparticles for the hydrogen evolution and oxygen reduction reactions

Benjamin Corona,^{a)} Marco Howard,^{a)} Liang Zhang, and Graeme Henkelman

Department of Chemistry and the Institute for Computational Engineering and Sciences, The University of Texas at Austin, Austin, Texas 78712-0165, USA

(Received 30 September 2016; accepted 28 November 2016; published online 30 December 2016)

Using density functional theory calculations, a set of candidate nanoparticle catalysts are identified based on reactivity descriptors and segregation energies for the oxygen reduction and hydrogen evolution reactions. Trends in the data were identified by screening over 700 core@shell 2 nm transition metal nanoparticles for each reaction. High activity was found for nanoparticles with noble metal shells and a variety of core metals for both reactions. By screening for activity and stability, we obtain a set of interesting bimetallic catalysts, including cases that have reduced noble metal loadings and a higher predicted activity as compared to monometallic Pt nanoparticles. *Published by AIP Publishing.* [http://dx.doi.org/10.1063/1.4972579]

I. INTRODUCTION

There is global interest in clean energy sources that would reduce our dependency on fossil fuels. Hydrogen fuel cells are one such example, but they are limited, particularly for vehicle applications, by the cost of current platinum catalysts. While the hydrogen evolution reaction (HER) is rapid on Pt, the oxygen reduction reaction (ORR) is sluggish and has a considerable over-potential.¹ Computational analyses have shown that while Pt is the optimal monometallic catalyst, it over-binds oxygen particularly for small Pt nanoparticles (NPs).^{2–4} Thus there is an opportunity to find better metal NP catalysts that are more active than Pt and more affordable if the loading of precious metals can be reduced.

Advances in computing resources and algorithms such as density functional theory (DFT) are now making the computational design of catalysts possible.⁵ Greeley and Nørskov, for example, have used a high throughput approach to explore near surface binary alloys with improved activity over Pt for the ORR and HER.⁶ They first predicted, and then experimentally verified, that a BiPt alloy has comparable activity to pure Pt for the HER. The Nørskov group also identified alloys that are active toward the ORR and found that the thermodynamic stability of surface alloys with a skin of Pd or Pt can be improved by the presence of a subsurface metal. Wang and Johnson⁷ showed by screening for segregation energies of binary transition metal nanoparticles that the stability of bimetallic NPs depends on the relative Wigner-Seitz radius and cohesive energies of the component metals.

Previous work in our group^{8–12} demonstrated the beneficial effects of alloying the core of core@shell and random alloy nanoparticles. Here we present a high-throughput study of 2 nm transition metal core@shell NPs for both the ORR and the HER. By exploring the landscape of potential catalysts, we

identify trends in activity and potential novel catalysts for both reactions.

II. METHODOLOGY

Calculations were performed using density functional theory (DFT) as implemented by the Vienna *ab initio* simulation package.^{13,14} Core electrons were described using the projector augmented wave method.¹⁵ Kohn-Sham single-electron wave functions were expanded in a plane wave basis with an energy cutoff of 274 eV to describe the valence electrons. The energy cutoff was increased to 400 eV to test for convergence, and the oxygen binding energy on Pt was found to vary by less than 0.01 eV. The generalized gradient approximation was used in the Perdew-Wang 91 functional¹⁶ to evaluate the exchange-correlation energy. All atoms in the structures were allowed to relax and NPs were considered converged when the force per atom was less than 0.01 eV/Å. Spin polarization was considered for all calculations.

The NPs were generated as 79 atom bimetallic face centered cubic (FCC) truncated octahedra with 19 core atoms and 60 shell atoms, as shown in Fig. 1. Each NP was converged in a box providing a typical vacuum gap of 8–10 Å between periodic images. Adsorbates were positioned in hollow sites on the (111) face of the NPs.^{17,18} Optimized structures were screened for deformation of one or more of the (111) faces. Particles with significant structural rearrangement were then excluded from the results.

Adsorbate binding energies for O and H were calculated as descriptors for the catalytic activity of the ORR and HER;¹⁹ segregation energies were calculated as a measure of stability.²⁰ The binding energies of oxygen and hydrogen, E_b^a ($a = O, H$), are given by $E_b^a = E_{\text{npa}} - E_{\text{bnp}} - E_a$, where E_{npa} and E_{bnp} are the energy of the NPs with and without adsorbates bound, respectively, and E_a is the reference energy of the adsorbate, which is taken to be half of the diatomic molecular energy.

^{a)}B. Corona and M. Howard contributed equally to this work.

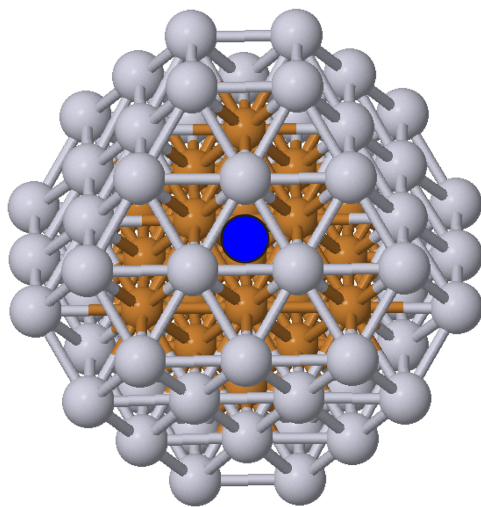


FIG. 1. Geometry of a 79-atom core@shell particle with the adsorbate binding site shown at the blue circle.

The activity for each reaction was determined from microkinetic models reported in the literature,^{5,6,21} the result of which is reproduced in the volcano plots in Fig. 2. Using the example of ORR, in the strong binding regime on the left side of the volcano, the reaction rate is limited by the release of oxygen species, while in the weak binding regime, the rate determining step becomes OOH formation.⁵

Segregation energies were calculated to estimate the thermodynamic stability of the NP in vacuum and in the chemical environment of the HER and ORR with H and O adsorbates bound to the surface. Previous studies have reported that an adsorbate can drive subsurface metals to the surface.²⁰ By calculating the segregation energy for both adsorbates, we were able to exclude nanoparticles with possible subsurface segregation from our list of the best candidates for synthesis. The

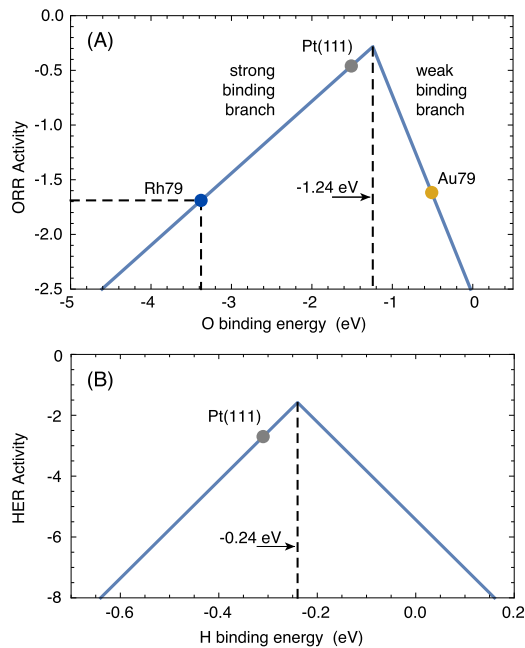


FIG. 2. Volcano plots, based upon microkinetic models in Refs. 5, 6, and 21, provide a correlation between adsorbate binding energies and reaction activities.

segregation energy, $E_{\text{seg}} = E_{\text{sbn}} - E_{\text{bnp}}$, was calculated by taking the difference in energy between a bare particle (E_{bnp}) and a particle with one core and shell atom exchanged (E_{sbn}). The thermodynamic stability of the NP under reaction conditions was estimated from the segregation energy in the presence of adsorbates. The segregation energy in the presence of an adsorbate was calculated in the same way as E_{seg} with both NP models having an adsorbate bound at the hollow site where the exchange of the shell and core atoms was done.

The best scenario for stability is for the particles to have positive segregation energies both in vacuum and under reaction conditions. Particles that are only stable under reaction conditions may also be suitable, whereas unstable particles are likely to undergo structural rearrangements and not show the predicted activity. We should note that this computational test of NP stability, while appropriate for rapid screening, is not comprehensive. Considering adsorbate coverage, as in a Pourbaix analysis, would be better. While this would determine thermodynamic stability, NPs could also be kinetically trapped in catalytically active structures, where the stability is hard to determine theoretically. It would therefore also be appropriate to suggest candidate NP catalysts from our rapid screening to experimentalists for the definitive determination of activity and stability.

III. RESULTS AND DISCUSSION

A. Oxygen reduction reaction

The activity of the core@shell NPs considered is shown in Fig. 3 and their stability in Fig. 4. Together, these charts can be used to identify candidate core@shell NPs for oxygen reduction. The activity plot shows that the shell metal is the dominant factor for catalytic activity. This is apparent from the greater variation across the columns of the activity chart as compared to the rows. Low activity on the chart is predominantly due to either a less noble (lower group) shell or a smaller period shell. In these cases, the low activity is due

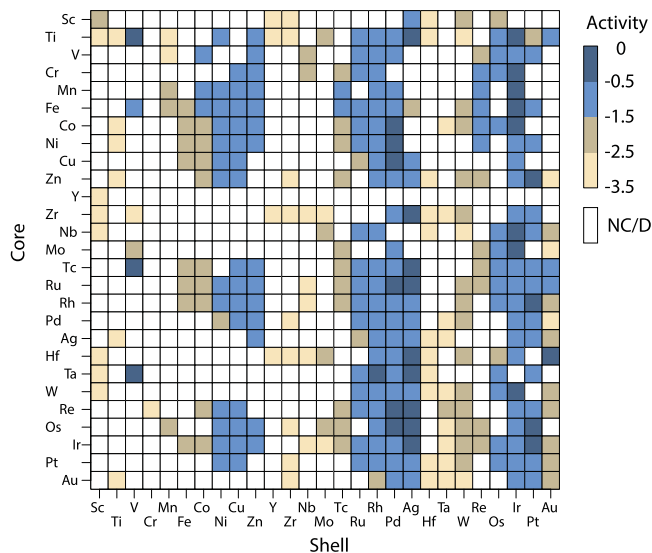


FIG. 3. Activity of core@shell NPs for the ORR. Higher activity corresponds to darker shades of color. NPs that did not converge or converged to deformed structures (NC/D) are colored white.

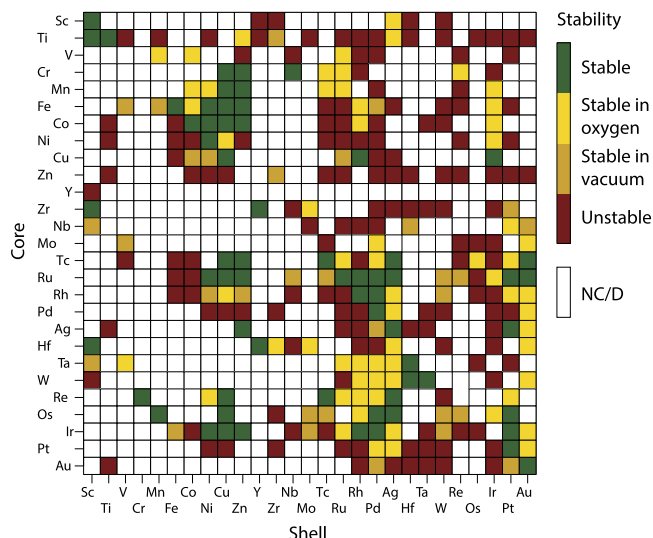


FIG. 4. Stability of core@shell NPs. NPs colored orange are stable with respect to swapping a core atom with a shell atom in vacuum; yellow are stable in oxidizing conditions, with O bound at the shell swap site; green are stable in both; and red in neither condition.

to oxygen binding on the strong-side of the volcano. Only in the case of Au shelled NPs was lower activity due to falling too far on the weak-binding side of the volcano. A significant difference was observed between the binding energies of 3d metals and 4d metals in group 10 and 11 shells and also between 3d and 5d metals. This difference disappeared in a t-test run between 4d and 5d shelled NPs. These results indicate that systematic tuning of the binding energy can be achieved by altering the shell metal. Most importantly, this result shows that catalysts with activity equal to or greater than Pt are typically limited to 4d and 5d metal shells in groups 9, 10, and 11.

As expected, Pt and Pd served as highly active shells for catalysis; alternative shell metals include Ag and Ir. Ag is particularly interesting because of the lower cost of Ag as compared to current Pt catalysts. The binding energy of Ag NPs lies close to the peak of the volcano, whereas bulk Ag is on the weak-binding branch. We should note, however, that Ag is known to dissolve in the acidic environments favored for fuel cell applications and so these candidates may only be appropriate in alkaline conditions. The increase in binding for NPs as compared to bulk can also be seen for Pt₇₉ which binds O at -1.77 eV as compared to -1.51 eV on a Pt slab. The other shell element that benefited from an increased binding in NP form was Au, but as we show, the activity is still too weak to produce a useful catalyst. In Table I, we have listed the top candidate Ag shell NPs that could be further investigated.

TABLE I. The top candidate NPs for the ORR. These particles have oxygen binding energies within 0.2 eV of the volcano peak, -1.24 eV, and are stable in both vacuum and an oxidizing environment.

Core@shell	O binding (eV)
{Ru,Re,Os,Tc}@Ag	-1.15, -1.22, -1.24, -1.29
{Os,Ir}@Pt	-1.18, -1.42
Ru@Pd	-1.43

As well as screening for adsorbate binding energy, we also investigated NP stability. This was done by calculating segregation energies of the NPs in vacuum, with an adsorbate bound, and by visually inspecting for deformation of one or more of the (111) binding faces. In general, deformation occurred more commonly in 3d metal shells, specifically among lower group metals. Within the 3d shell metal columns, atomic radius of the core metal was a good predictor of deformation. Group 6 and greater core metals proved to be less likely to deform in the 3d shells compared to group 3 metals like Y and Sc. Similar to the deformation screening, segregation energy calculations significantly reduced the number of candidate NPs with high activity and stability. While many NPs were unstable in both configurations, there was a general trend of stability along the diagonal of the figure. These stable candidates often have cores with less full valence shells (which are represented as cells slightly above the diagonal). These stable core atoms tended to be cores that were in the middle of the d-block such as Mn, Fe, Ru, Os, and Ir.

Based on the screening of activity, deformation, and stability, it was possible to identify a variety of NPs that fit all of the criteria for being a stable catalyst; these results are presented in Table I.

B. Hydrogen evolution reaction

The window for acceptable binding energies in HER was tighter due to the steeper slopes in the volcano plot. To account for this, the activity ranges of interest were widened. Any NP with an activity above -5 (blue colored entries in Fig. 5) was considered a potential candidate for catalysis. Similar to the ORR, the nobility of the shell plays a primary role in determining the activity of the NP. Shells from within groups 8, 9, and 10 exhibited the best activity while other NP shells bound H too tightly. Also, as with ORR, Au is not active, but

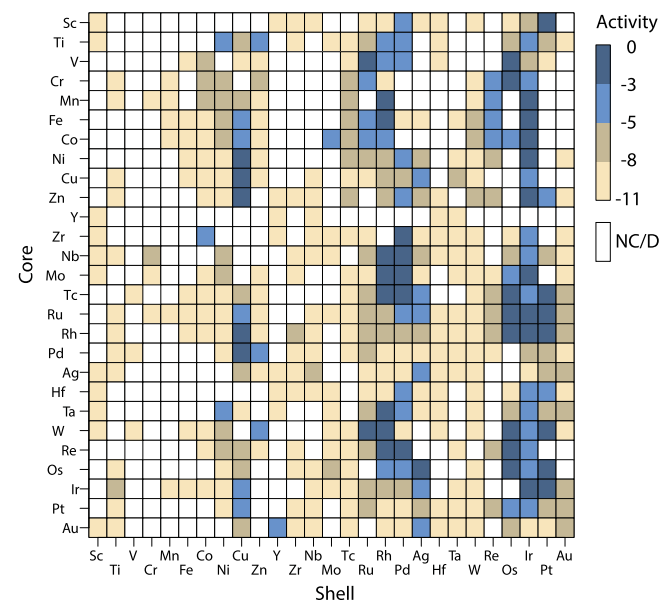


FIG. 5. HER activity of core@shell NPs. The vertical trends are clear as well as certain core elements that reduce the activity of shells that are generally active, including Y, Zr, Hf, and Au.

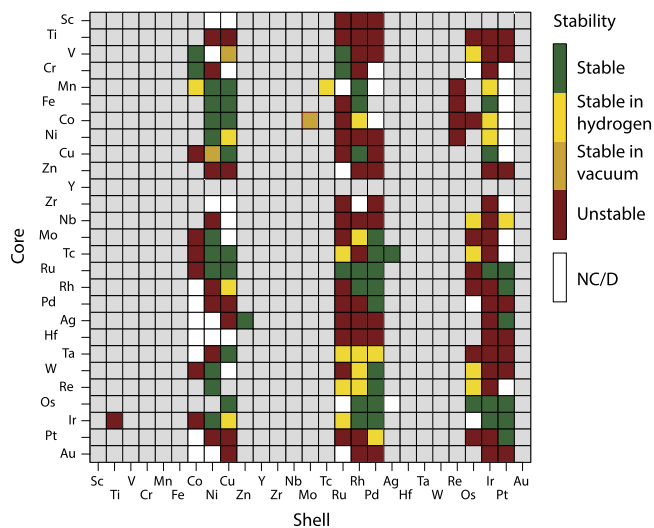


FIG. 6. Stability of NPs both in vacuum and in a hydrogen environment. Note that the stability of particles that were found not to be active for HER was not calculated (marked as grey).

unlike ORR, the set of Ag-shelled NPs provided only one candidate in the most active category. Cu provided multiple active candidates, which is of interest because Cu is cheaper than other candidates including Pd and Pt that are known to have high HER activities. Unlike ORR, certain core elements play a significant role in the HER by reducing the activity of their respective NPs. Ag and Au cores, for example, gave rise to inactive NPs nearly regardless of shell. In a similar manner, metals from the left side of the d-block such as Sc, Y, Zr, and Hf all contributed to either reduced activity or deformation of the NP.

The stability of NPs for HER is shown in Fig. 6. Once again, Pt and Pd shelled NPs were the only stable candidates that had cores with binding energies on either side of the volcano peak and thus allow for alloy tuning of the core. Due to the smaller size and electronegativity of the adsorbate molecule, fewer NPs were found to deform upon adsorbate binding. The result of elements with large radii not fitting in 3d element shells was consistent to what was found for ORR. Moving toward the right of the graph, however, deformity was less frequent. Considering both activity and stability developed, Table II shows our best candidates for synthesis.

TABLE II. The top candidate core@shell NPs for the HER bind hydrogen within 0.1 eV of the volcano peak, -0.24 eV, which are stable in both vacuum and a reducing environment.

Core@shell	H binding (eV)
{Ru,Os,Ir,Rh}@Pt	$-0.17, -0.18, -0.25, -0.26$
{Tc,Mo,Re}@Pd	$-0.19, -0.27, -0.28$
{Fe,Ir,Ru}@Ir	$-0.24, -0.31, -0.27$
{Fe,Mn}@Rh	$-0.30, -0.24$
V@Ru	-0.28
Os@Os	-0.30
Cu@Cu	-0.32

IV. CONCLUSION

High-throughput screening of activity and stability showed trends across hundreds of core@shell bimetallic NPs. The top candidates listed in Tables I and II for the ORR and HER are calculated to be stable under reaction conditions and active as compared to a Pt(111) reference.

ACKNOWLEDGMENTS

We gratefully acknowledge support from the National Science Foundation (Grant No. CHE-1534177), the Welch Foundation (Grant No. F-1841), the Freshman Research Initiative, and computational resources from the Texas Advanced Computing Center.

- ¹N. P. R. Markovic and P. Ross, "New electrocatalysts for fuel cells from model surfaces to commercial catalysts," *CATTECH* **4**, 110–126 (2000).
- ²J. Greeley, J. K. Nørskov, L. A. Kibler, A. M. El-Aziz, and D. M. Kolb, "Hydrogen evolution over bimetallic systems: Understanding the trends," *ChemPhysChem* **7**, 1032–1035 (2006).
- ³J. K. Nørskov, T. Bligaard, J. Rossmeisl, and C. H. Christensen, "Towards the computational design of solid catalysts," *Nat. Chem.* **1**, 37–46 (2009).
- ⁴W. Tang and G. Henkelman, "Charge redistribution in core-shell nanoparticles to promote oxygen reduction," *J. Chem. Phys.* **130**, 194504 (2009).
- ⁵J. K. Nørskov, J. Rossmeisl, A. Logadottir, L. Lindqvist, J. R. Kitchin, T. Bligaard, and H. Jonsson, "Origin of the overpotential for oxygen reduction at a fuel-cell cathode," *J. Phys. Chem. B* **108**, 17886–17892 (2004).
- ⁶J. Greeley, T. F. Jaramillo, J. Bonde, I. B. Chorkendorff, and J. K. Nørskov, "Computational high-throughput screening of electrocatalytic materials for hydrogen evolution," *Nat. Mater.* **5**, 909–913 (2006).
- ⁷L.-L. Wang and D. D. Johnson, "Predicted trends of core-shell preferences for 132 late transition-metal binary-alloy nanoparticles," *J. Am. Chem. Soc.* **131**, 14023–14029 (2009).
- ⁸W. Tang, L. Zhang, and G. Henkelman, "Catalytic activity of Pd/Cu random alloy nanoparticles for oxygen reduction," *J. Phys. Chem. Lett.* **2**, 1328–1331 (2011).
- ⁹D. F. Yancey, L. Zhang, R. M. Crooks, and G. Henkelman, "Au@Pt dendrimer encapsulated nanoparticles as model electrocatalysts for comparison of experiment and theory," *Chem. Sci.* **3**, 1033–1040 (2012).
- ¹⁰L. Zhang and G. Henkelman, "Tuning the oxygen reduction activity of Pd shell nanoparticles with random alloy cores," *J. Phys. Chem. C* **116**, 20860–20865 (2012).
- ¹¹L. Zhang, R. Iyyappaperumal, D. F. Yancey, R. M. Crooks, and G. Henkelman, "Design of Pt-shell nanoparticles with alloy cores for the oxygen reduction reaction," *ACS Nano* **7**, 9168–9172 (2013).
- ¹²L. Zhang and G. Henkelman, "Computational design of alloy-core@shell metal nanoparticle catalysts," *ACS Catal.* **5**, 655–660 (2014).
- ¹³G. Kresse and J. Hafner, "First-principles study of the adsorption of atomic H on Ni(111), (100) and (110)," *Surf. Sci.* **459**, 287–302 (2000).
- ¹⁴G. Kresse, "Dissociation and sticking of H₂ on the Ni(111), (100), and (110) substrate," *Phys. Rev. B* **62**, 8295 (2000).
- ¹⁵P. E. Blöchl, "Projector augmented-wave method," *Phys. Rev. B* **50**, 17953–17979 (1994).
- ¹⁶J. P. Perdew and Y. Wang, "Accurate and simple analytic representation of the electron-gas correlation energy," *Phys. Rev. B* **45**, 13244 (1992).
- ¹⁷S. López-Moreno and A. H. Romero, "Atomic and molecular oxygen adsorbed on (111) transition metal surfaces: Cu and Ni," *J. Chem. Phys.* **142**, 154702 (2015).
- ¹⁸W.-X. Li, C. Stampfl, and M. Scheffler, "Oxygen adsorption on Ag(111): A density-functional theory investigation," *Phys. Rev. B* **65**, 075407 (2002).
- ¹⁹T. Bligaard, J. K. Nørskov, S. Dahl, J. Matthiesen, C. H. Christensen, and J. Sehested, "The Brønsted–Evans–Polanyi relation and the volcano curve in heterogeneous catalysis," *J. Catal.* **224**, 206–217 (2004).
- ²⁰J. Greeley and M. Mavrikakis, "Alloy catalysts designed from first principles," *Nat. Mater.* **3**, 810–815 (2004).
- ²¹J. K. Nørskov, T. Bligaard, A. Logadottir, J. R. Kitchin, J. G. Chen, S. Pandelov, and U. Stimming, "Trends in the exchange current for hydrogen evolution," *J. Electrochem. Soc.* **152**, J23–J26 (2005).